BETA SPECTROMETRY
PERFORMANCE OF A VOYAGER DETECTOR
FOR MAGNETOSPHERIC ELECTRONS

by Minh Q. Tran
Sponsored by John F. Cooper, Ph.D.
CALIFORNIA INSTITUTE OF TECHNOLOGY

Internal Report #96

BETA SPECTROMETRY
PERFORMANCE OF A VOYAGER DETECTOR FOR MAGNETOSPHERIC ELECTRONS

Minh Q. Tran
Summer Undergraduate Research Fellowship, 1987
Project Sponsor: Dr. John F. Cooper
California Institute of Technology
Pasadena, CA 91125

ABSTRACT

Due to large uncertainties in the electron measurements taken by the Caltech Cosmic Ray System (CRS) in a high electron intensity of the Uranus magnetosphere during the recent encounter of the spacecraft Voyager with the planet, a laboratory calibration of two detectors identical to those used in the Electron Telescope (TET) and the Low Energy Telescopes (LETs) was carried out. The electron response of these detectors was measured with a beta spectrometer experiment below the beta decay end point energy (3.54 MeV) of a Ru^{106} source and at various incidence angles from 0^o to 60^o. The TET's 3mm detector (D1) showed a $\geq$ 80 % electron efficiency up to 1.4 MeV and dropped off thereafter due to detector penetration. In comparison, the LETs' 450μm detector (L3) showed $\geq$ 70 % response only up to 350 KeV. We also looked at the energy deposit distribution in the detectors and the effects on the distribution of varying electron energy and incidence angle. The observed effects were found to be consistent with theoretical expectations. These measurements can now be used to understand complicated detector response phenomena such as possible electron pile-up in the inner magnetosphere of Uranus.

Introduction

On January 24, 1986, the spacecraft Voyager 2 encountered Uranus. Among the experimental equipment on spacecraft was the Caltech Cosmic Ray System (CRS), designed to measure energetic electrons, protons, and ions. High intensities of energetic electrons in the KeV to MeV range trapped in the planet's magnetosphere were found. In this high intensity magnetospheric environment, possible problems with detector deadtime and electron pulse pile-up can occur. Such problems can modify the data obtained, and thus they should be investigated. This work carried out an initial laboratory investigation of the electron efficiencies of two CRS electron detectors which showed signficant response to electrons in the Uranus magnetosphere. The efficiency of the detectors were obtained at various energies and incidence angles with a magnetic spectrometer.

Apparatus

The detectors calibrated were a Lithium-drifted silicon detector of 4.5 cm^2 center active area and 3 mm thickness (which is referred to as D1) and a surface barrier silicon detector of 4.5 cm^2 active area and 450 μm thickness (referred to as L3). The thicker D1 detector is more efficient at counting electrons, whereas the thinner L3 detector is primarily used for counting heavier charged particles like protons and ions. The D1 detector has on one side a dead layer of a few hundred μm in thickness, which reduces its depletion width, and on the other side an aluminum evaporated surface corresponding to a few μm of silicon. The L3 detector has on both sides an aluminum evaporated surface. Normal operation required that the detectors be biased to their operating voltages–500 volts for the D1 and 200 volts for the L3. If low pressure operation is necessary, the detector should never be biased in the pressure region from 10 μm to several mm Hg.

The laboratory spectrometer consists of a Ru^{106} beta source placed in a magnetic field generated by an electromagnet, a beam exit hole, and a tiltable and movable detector mount, all inside a high vacuum chamber. The detector (D1 or L3) is placed on the mount with the negligibly thick aluminum side facing the electron beam. Pressure inside the chamber is reduced by a two stage evacuation process, first with a mechanical pump and then with a cryogenic pump. The beam energy is controlled by the magnetic field, which is measured with a gauss meter. See Figure 1 for a schematic description of the spectrometer and the appendix for a table tabulating the magnetic field strengths and the corresponding beam energy. The detector is biased by a high voltage source according to its specification.

Charged particles hitting the detector create free electrons by atomic ionization which are collected by a charge sensitive pre-amplifier, amplified and fed through a discriminator to a pulse height analyzer (PHA). The PHA records the spectrum of energy deposited by the charged particles. It is calibrated with a pulse generator which outputs pulses of known pulse heights. Data recorded by the PHA are transfered to a VAX computer and stored before analyzed.

Procedure

a) Lab Work

Because the range of an electron in air at atmospheric pressure is a few centimeters, the spectrometer chamber was evacuated to 10^{-3} torr with a mechanical pump and then to 10^{-6}-10^{-5} torr ($\sim 10^{-3}$-10^{-2} atm) with a cryogenic pump. After reaching this pressure, the detector is biased to its operating voltage. Since the beam is non-uniform and its cross section is larger than the detector active area, the detector is placed at the optimum position in the beam where the largest number of electrons is counted and where the detector response is least sensitive to the beam position. In figure 1, the optimum position is B. The spectrometer electromagnet is then turned on, providing a magnetic field guiding almost-monoenergetic beta particles from the source to the exit hole. The beta beam is not completely monoenergetic because of the large width of the exit hole, a rectangular slit 1 cm wide.

To confirm that the detector primarily detects β-rays from the source, the rates of electrons, i.e. the number of electrons detected over the detector live time were counted and checked against theory. Figure 2 shows the experimental points plotted together with the theoretical beta decay electron intensity

$$I(T) = k(T + M)^2(T_{max} - T)^2$$

where $I(T)$ is the intensity of electrons of kinetic energy T and rest mass $M = m_0c^2$, T_{max} is the electron's maximum kinetic energy, which is unique to a source, and k is a normalization constant, which is taken to be the maximum value of the total number of electrons passing through the detector 0.9in-diameter active area. The beta source used for this experiment was Ru^{106} with $T_{max} = 3.54$ MeV. The slight discrepancies between theory and experiment can be accounted for by the geometry of the beam. A non-uniform beam can be the cause of the discrepancies. Over all, however, it is safe to assume that what the detector detects is mostly electrons.

b) Definition of Efficiency

Since primary purpose of this project was to determine the efficiency of the detector as the electron energy and incidence angle vary, I will discuss the method for measuring the detector efficiency. But first, it is helpful to discuss the electron detection process within a detector and the energy loss distribution before defining how the efficiency is measured.

As an electron, or more generally, a charged particle, passes through the detector, it deposits energy by ionizing the material of which the detector is made. If the particle is stopped within the detector, its initial kinetic energy is totally deposited. If it escapes, only a fraction is deposited. Thus, the detector is less efficient at recording the energy of faster particles than slower particles. A beam of monoenergetic electrons is therefore recorded as a distribution, which is also nearly monoenergetic only if all electrons stop in the detector.

Figure 3 shows an electron energy loss distribution with its features labeled. The peak corresponds to electrons with the full energy of the beam, 970 KeV. The spread in energy, 96 KeV, shown in the width of the peak is due to the large slit size as well as to intrinsic electronic noise in the detector and associated electronics. The total number of electrons detected is the integral of the distribution. The "tail" region corresponds to those 970 KeV electrons that deposited only from 370 to 850 KeV instead of their full energy in the peak. The efficiency of the detector is defined to be the integral of the full energy peak divided by the total number detected.

Results

a) Efficiency at normal incidence

Table 1 gives the laboratory calibrated values of the electron detection efficiency at normal incidence of the 3mm detector with 500 KeV threshold, the same as that of the TET D1 detector. Figure 4 shows a plot of these values. The efficiency stays above 80% for energies $\geq$ 1.4 MeV but thereafter decreases more rapidly. Efficiencies at energies greater than 2.9 MeV were not obtainable due to the current limitation of the electromagnet.

Table 2 gives the corresponding efficiency of the 450μm (L3) detector. The discriminator threshold was set at 115 KeV, just above the noise level. A plot of these values is shown in figure 5. Because the data points above 400 KeV, the detector penetration

TABLE 1

Efficiency of 3mm Detector, threshold=500 KeV

Energy (KeV)	Efficiency (%)
632 ± 8	96.6 ± 1.0
984 ± 8	85.6 ± 0.8
1367 ± 8	80.0 ± 0.7
1758 ± 8	66.7 ± 0.6
2173 ± 8	41.9 ± 0.5
2564 ± 16	24.0 ± 0.5
2940 ± 24	13.9 ± 0.6

TABLE 2

Efficiency of 450μm detector, threshold=115 KeV

Energy (KeV)	Efficiency (%)
131 ± 8	81.97 ± 6.99
147 ± 8	97.09 ± 3.07
290 ± 8	83.47 ± 1.44
314 ± 8	78.59 ± 1.28
354 ± 8	69.81 ± 1.09
378 ± 8	67.88 ± 1.06
418 ± 8	51.76 ± 0.78
450 ± 8	42.36 ± 0.66
474 ± 8	34.33 ± 0.56
513 ± 8	26.84 ± 0.46
537 ± 8	22.30 ± 0.40
577 ± 8	18.61 ± 0.35
617 ± 8	13.09 ± 0.28
705 ± 8	7.73 ± 0.20
792 ± 16	3.77 ± 1.37
864 ± 16	2.15 ± 1.01
968 ± 16	1.00 ± 0.68
1079 ± 24	0.621 ± 0.05
1143 ± 24	0.334 ± 1.95

energy, seem to indicate that the efficiency follows an exponential relation with respect to the energy, they were fitted to an exponential curve. Figures 6 and 7 seems to confirm this exponential-relation hypothesis. The e-folding energy is 145 KeV which corresponds to a scattering mean free path of about 100 μm for secondary electrons stopping in the detector volume. It should also be mentioned that not enough data were taken to verify

this relation for the D1 detector.

b) Efficiencies at other incidence angles

The efficiency of the D1 detector at various incidence angles are tabulated in Table 3. There are two observations from Table 3: 1) For energies $\leq$ 1774 KeV, the efficiency shows a decreasing trend as the incidence angle increases. 2) For energies $\geq$ 2565 KeV, the efficiency increases as the incidence angle increases.

TABLE 3

Efficiency at various angles of incidence

Beam Energy (KeV)	Angle (Degrees) 0	10	20	40	60
620±8	96.6±1.0	94.5±1.1	94.8±1.1	93.3±1.3	94.0±1.8
984±8	85.6±0.8	83.0±0.8	83.3±0.8	80.0±0.9	77.3±1.2
1363±8	80.0±0.7	79.6±0.7	76.9±0.7	73.4±0.8	67.3±0.9
1774±8	66.7±0.6	61.8±0.6	62.5±0.7	59.9±0.7	56.4±0.8
2162±8	41.9±0.5	40.3±0.5	41.4±0.6	43.8±0.6	42.4±0.8
2565±16	24.0±0.5	23.6±0.5	25.8±0.5	31.2±0.7	30.1±0.8
2754±24	13.9±0.6	13.8±0.6	15.5±0.6	20.3±0.8	17.9±1.0

The first can be understood by backscattering. As an electron hits the detector, there is a finite probability that it will backscatter and not penetrate deeply into the detector. This probability increases with increasing incidence angle and decreases with increasing incidence energy. Electrons with low energy and high incidence angle will therefore backscatter more often, penetrating only a small distance into the detector and depositing only a small amount of their initial energy. The second observation is accounted for by the larger path length through the detector, since the detector efficiency is sensitive to pathlength at these energies for forward-scattering

c) The Energy Loss Distribution

The measured distributions of energy loss can be discussed qualitatively in terms of the physics of electron interactions in the detectors. Figures 8, 9, 9B, 10, 10B, 11, and 11B show the distributions of 1760, 2170, 2560, and 2940 KeV electrons, respectively. The tail of the distributions exhibits a change as the beam energy is increased. At 1760 KeV, the tail is relatively flat. However, at higher energies the tail grows in proportion to the

full-energy peak and becomes a "peak" itself. The distribution around this peak, called the most probable peak, is called a Landau distribution for very thin detectors, in which incident electrons lose a negligible fraction of their energy, and a Vavilov distribution for thicker detectors. In the limit of a very thick detector, in which all electrons stop, the distribution would be Gaussian. Compared with a distribution seen earlier in figure 3 the low energy tail of the Vavilov distribution becomes significant at high energy when the electrons escape from the detector, depositing only a fraction of their energy. It turns out that many electrons lose a specific amount of energy passing through a detector regardless of their full energy. Notice also the asymmetric shape of the distribution.

The shape of these distributions can be explained straightforwardly. Charged particles passing through a slab of material of a certain thickness lose on the average a specific amount of energy which is proportional to this thickness. Thus, as long as the charged particles have sufficient energy to go through the slab of material, they lose this specific amount of energy. For the 3mm detector, it is about 1.1 MeV. The presence of the full-energy peak indicates that a fraction of the number of electrons passing through is scattered in such a way that their paths inside the detector are longer than the detector thickness so that the number of encounters with the target atoms is large. Of course, these paths have to be sufficiently long so that they can deposit all of their energy.

The asymmetric shape of the energy loss distribution for relatively thin detectors can be understood by a phase space argument. An electron passing by a target atom loses more energy when it comes closer to the atom than when it is far from the atom. In the figure below A is the region of high energy loss, and B the region of low energy loss.

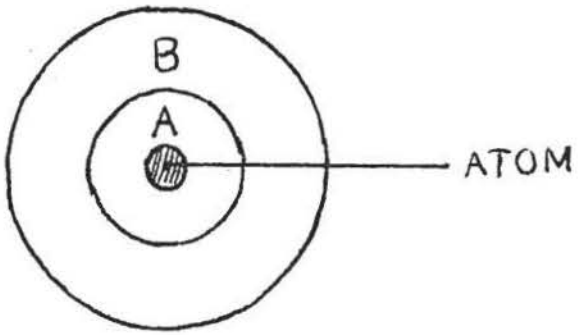

Since the area of region A is smaller than the area of region B the probability of large energy loss is smaller than the probability of small energy loss. This phenomenon accounts for the drop-off to the right of the most probable peak. The position of the most probable

peak corresponds to a characteristic impact parameter. Beyond this distance of approach the interaction of the electron and the nucleus becomes very small. The steep region to the left of the most probable peak is attributed to the interaction of delta rays, which are secondary electrons produced when target atoms are ionized. Since the delta rays produced have lower energy they deposit less energy than the primary (beam) electrons.

e) Shift of Most Probable Peak

As the detector is tilted to large incidence angles, the effective thickness of the detector increases. Thus one expects that the most probable peak will move closer to the main peak. Indeed, this shift upward is observed for the 3mm detector:

θ (deg.)	10	20	40	60
Energy (KeV)	1060±100	1100±80	1240±100	1350±100

This shift, however, does not follow the simple $\sec(\theta)$ relation and needs further investigation. Factors to be considered are the non-uniformity of the beam intensity, and the dead layer's thickness. A map of the beam intensity has been obtained at various energies and at detector positions 1 centimeter apart. Still, a more detailed map is needed, since the detector's active area is about 0.9 inch in diameter.

Conclusions

The detector efficiency was expected to decrease with increased electron energy. The D1 detector showed an efficiency higher than 80% for energy $\leq$ 1.4 MeV. In comparison, the L3 showed a 70% or higher efficiency at 350 Kev and less. An exponential drop was observed for the L3 detector, but has not been confirmed with the D1 detector due to insufficient data. As the incidence angle increased, the efficiency of the D1 detector decreased at energies below 1.8 MeV, but increased at energies above 2.5 MeV. The angular dependence can be explained by backscattering at low energies and by forward scattering and larger path lengths at higher energies.

In the course of obtaining the laboratory-calibrated efficiency of the D1 detector in the energy range 0.5 - 3 MeV range, the most probable peak was observed at 1.060 MeV at beam energy $\geq$ 2.1 MeV. As the incidence angle, hence the effective thickness of the detector, was increased the most probable peak shifted from 1.060 to 1.350 MeV.

The electron efficiency data can now be used to enhance interpretation the data obtained by the Caltech Cosmic Ray System in the planetary magnetospheres of Jupiter, Saturn, and Uranus and will also be invaluable for the upcoming Voyager 2 encounter with Neptune in August 1989. With these laboratory data the intensities of electrons incident on the CRS detectors can be calculated quantitatively, and possible effects of electron pile-up at high intensities can be studied.

Acknowledgement

This work is supported by a Caltech 1987 IBM SURF fellowship. I would like to thank Dr. John F. Cooper, my project sponsor, for his insights, advices, and suggestions throughout the course of the project. I would like to give special thanks to Dr. Alan Cummings for providing me with the research opportunity leading to the project, to Jim Weger and Dan Burke for their help with the electronic setup, and to Eric Christian for his helpful discussion.

Appendix

The table below gives the values of the spectrometer magnetic field strengths and their corresponding energies.

Magnetic Field Strength vs. Beam Energy

B (gauss) $\pm$ 5	T (KeV)
200	162 $\pm$ 8
400	454 $\pm$ 8
500	632 $\pm$ 8
700	984 $\pm$ 8
900	1367 $\pm$ 8
1000	1577 $\pm$ 8
1100	1758 $\pm$ 8
1200	1988 $\pm$ 8
1300	2173 $\pm$ 8
1400	2357 $\pm$ 16
1500	2564 $\pm$ 16
1600	2754 $\pm$ 24
1700	2940 $\pm$ 24

Spectrometer Beam Characteristics

The motion of a charged particle moving in a uniform, constant magnetic field can be described by

$$p_n = 3.00 \times 10^{-4} Ba$$

where p_n is the particle's momentum component normal to the field (in MeV/c), B is the field strength (in gauss), and a is the radius of curvature (in cm). With an effective radius $a = 5.95$ cm from the beta spectrometer notes in the lab,

$$p_n = 1.785B$$

The plots of p versus B for both detectors (D1 and L3) are on the next pages. Here p is the total momentum, not just the normal component p_n. For the particles measured with the D1 detector,

$$p = (12.4 \pm 7.4) + (2.01 \pm 0.007)B,$$

and for those measured with the L3 detector,

$$p = (49.9 \pm 8.6) + (1.90 \pm 0.02)B$$

Compared to 1.785, the factor multiplying B is larger, suggesting a larger radius of curvature or a smaller normal-component momentum. This is only possible if the motion of the electrons has a momentum component parallel to the magnetic field's direction. In other words, the particles follow a helical motion instead of a circular motion.

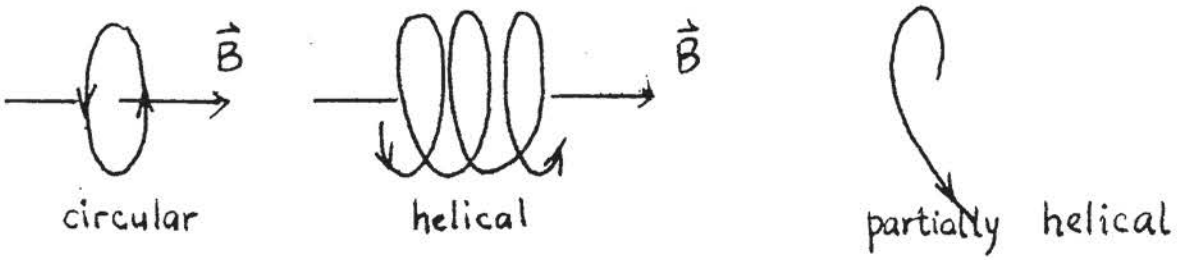

The helical path, although only partical due to the localized distribution of the field, is confirmed by the position of the beam with respect to the position of the collimator exit hole. The beam was found to be 3 cm north and 1 cm east of the center of the collimator slit at the position where the the detector was mounted, i.e. 6 inches above the exit hole.

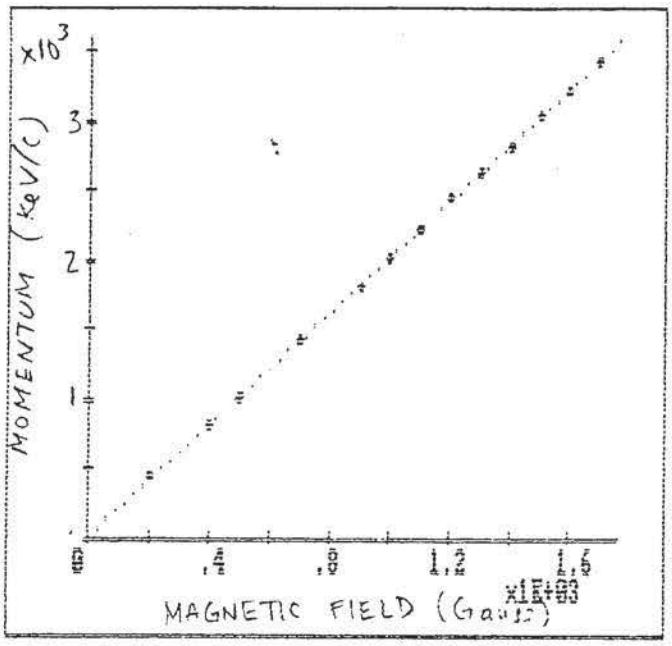

a:dimoment.dat

XOFF = 0
DX = 200
YOFF = 0
DY = 500

Y = A+B*X
(N = 13)
A = 12.54545
SIG(A) = 7.411998
B = 2.818828
SIG(B) = .0071544
CHI^2/(N-2) = 1.6246875

momentum (Kev/c) vs. magnetic field (gauss)--D1

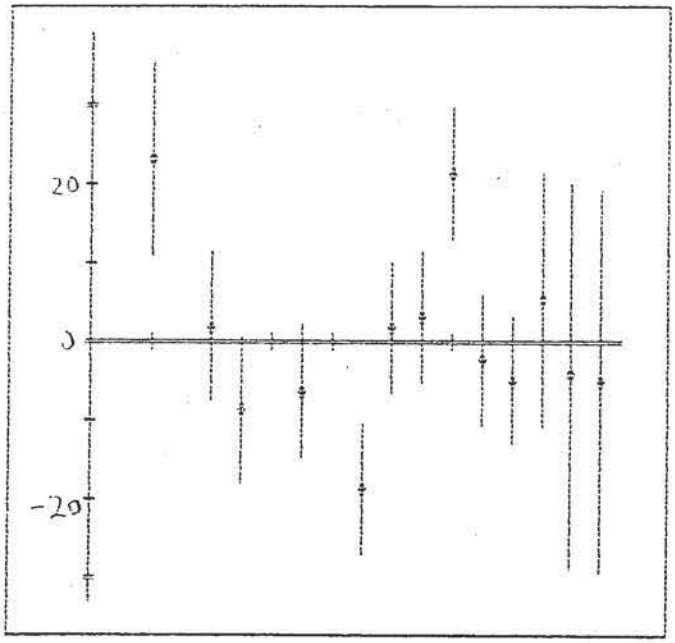

a:dimoment.dat

XOFF = 0
DX = 200
YOFF = 0
DY = 10

momentum (Kev/c) vs. magnetic field (gauss)--D1--difference plot

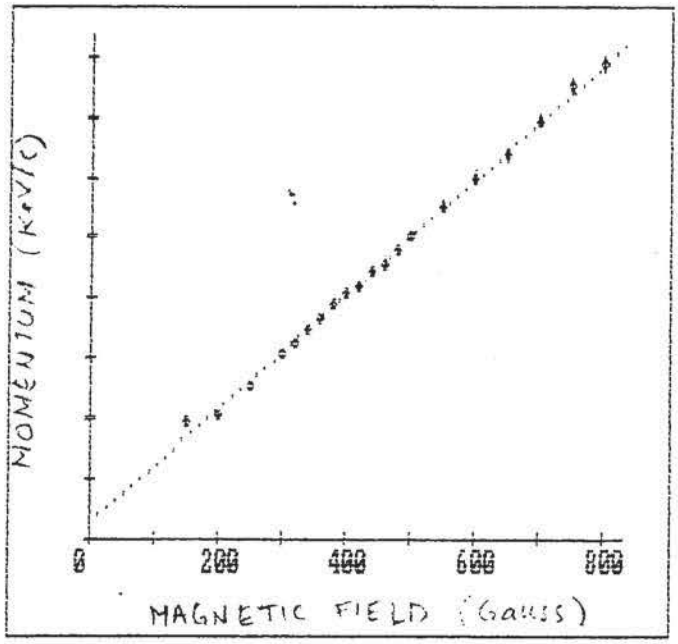

a:momentum.dat

XOFF = 0
DX = 100
YOFF = 0
DY = 200

Y = A+B*X
(N = 20)
A = 49.91129
SIG(A) = 8.641479
B = 1.901608
SIG(B) = 2.043583E-02
CHI^2/(N-2) = 1.392689

momentum (Kev/c) vs. magnetic field (gauss)--L3

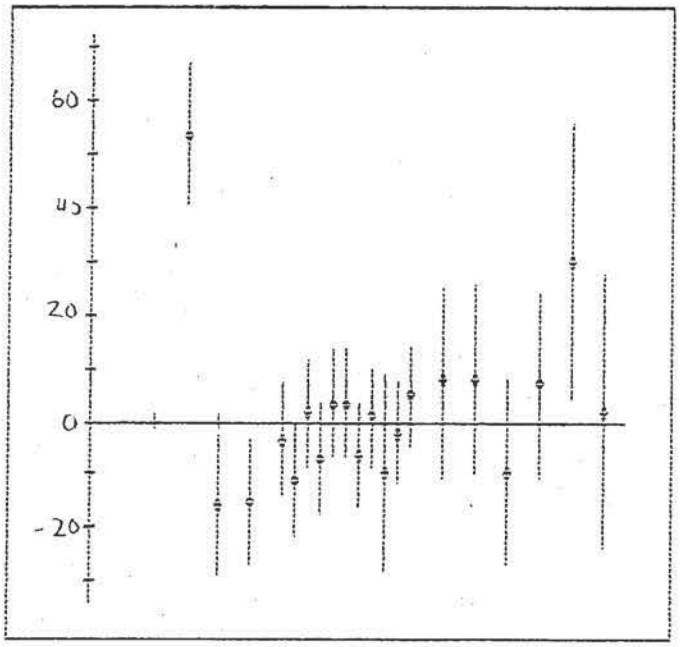

a:momentum.dat

XOFF = 0
DX = 100
YOFF = 0
DY = 10

momentum vs. magnetic field -- L3 -- difference plot

FIGURE 1: SCHEMATIC OF SPECTROMETER

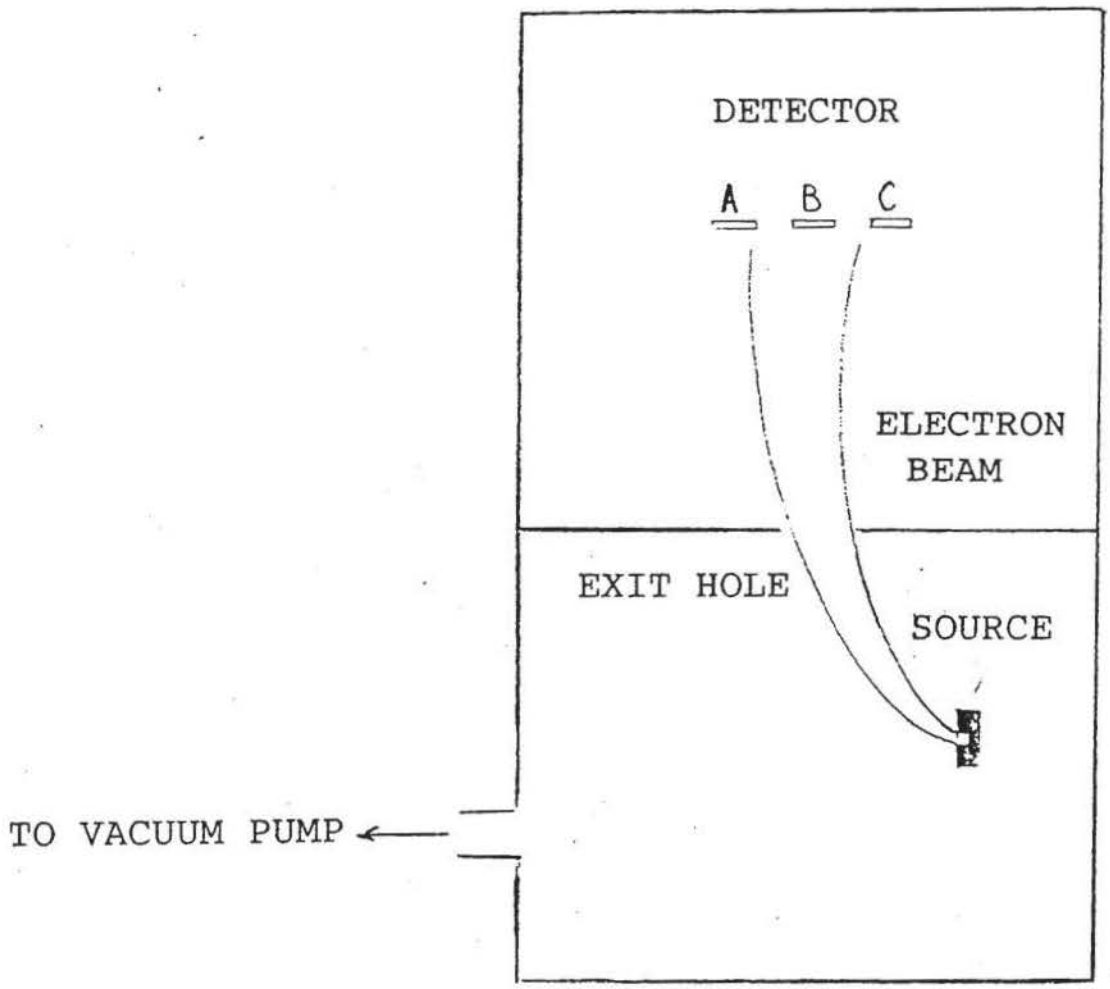

FIGURE 2: ELECTRON COUNTS IN 3 MM DETECTOR: THEORETICAL VS. EXPERIMENTAL

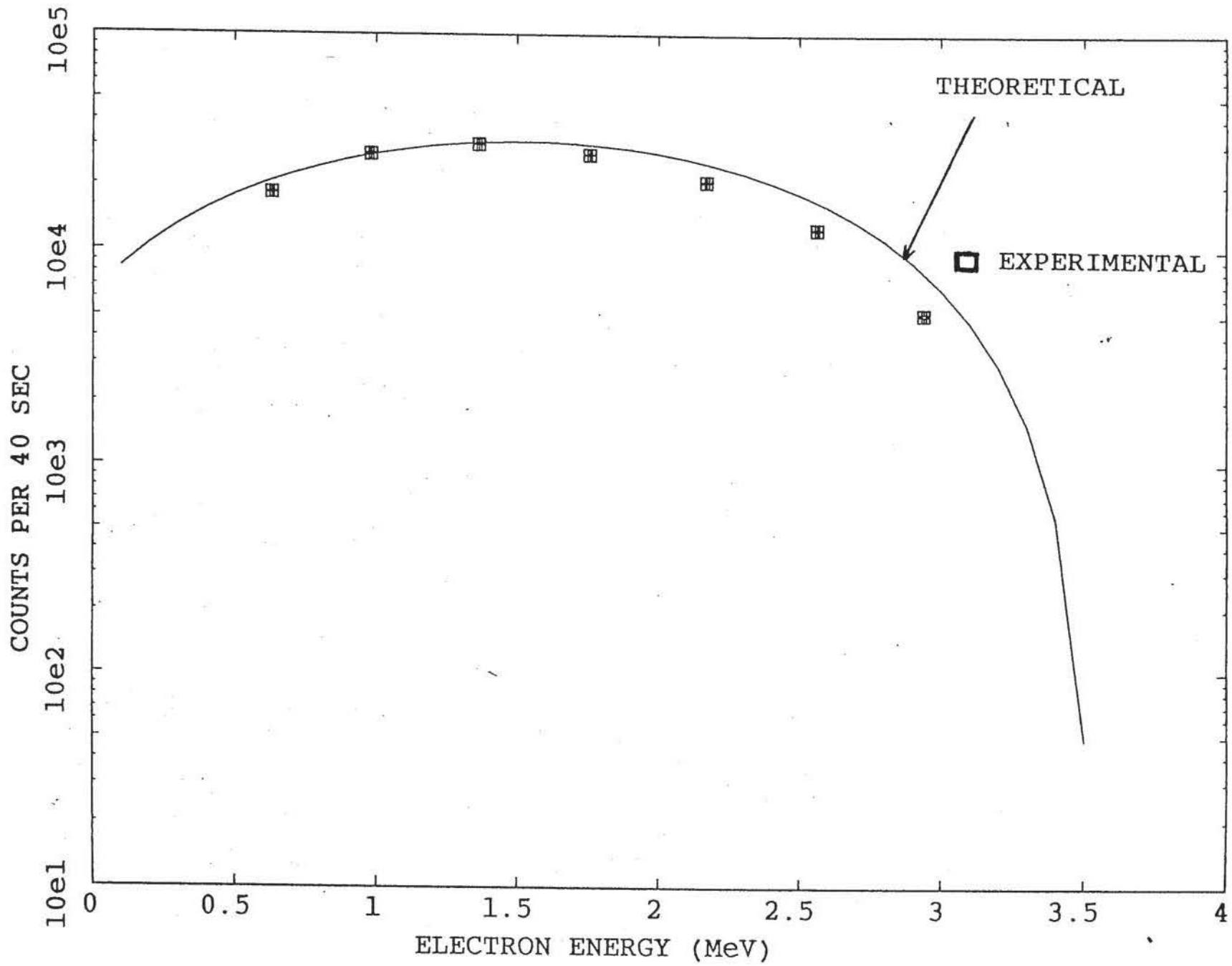

FIGURE 3: ELECTRON ENERGY LOSS DISTRIBUTION IN 3 MM DETECTOR

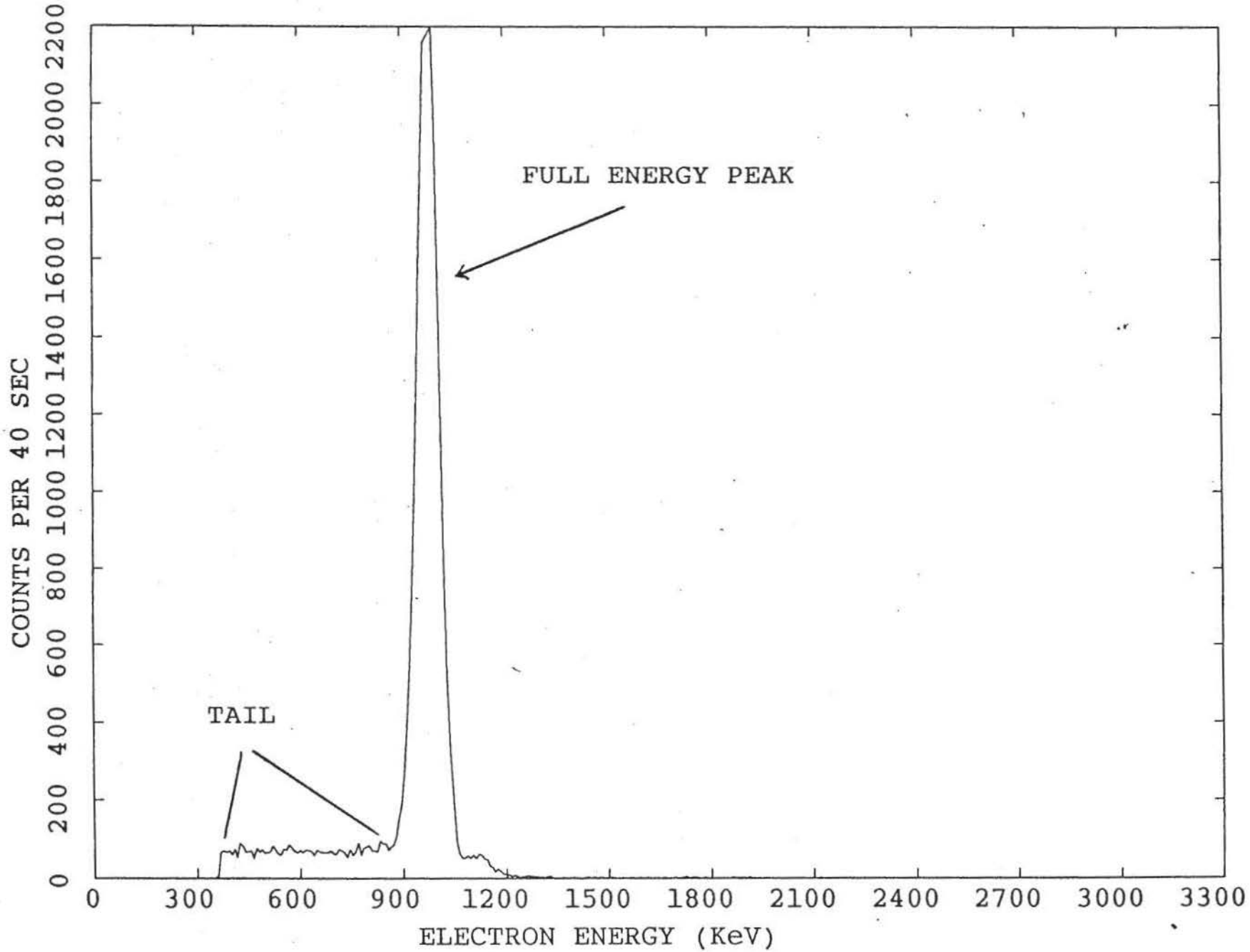

FIGURE 4: EFFICIENCY OF 3 MM DETECTOR (THRESHOLD=500KEV)

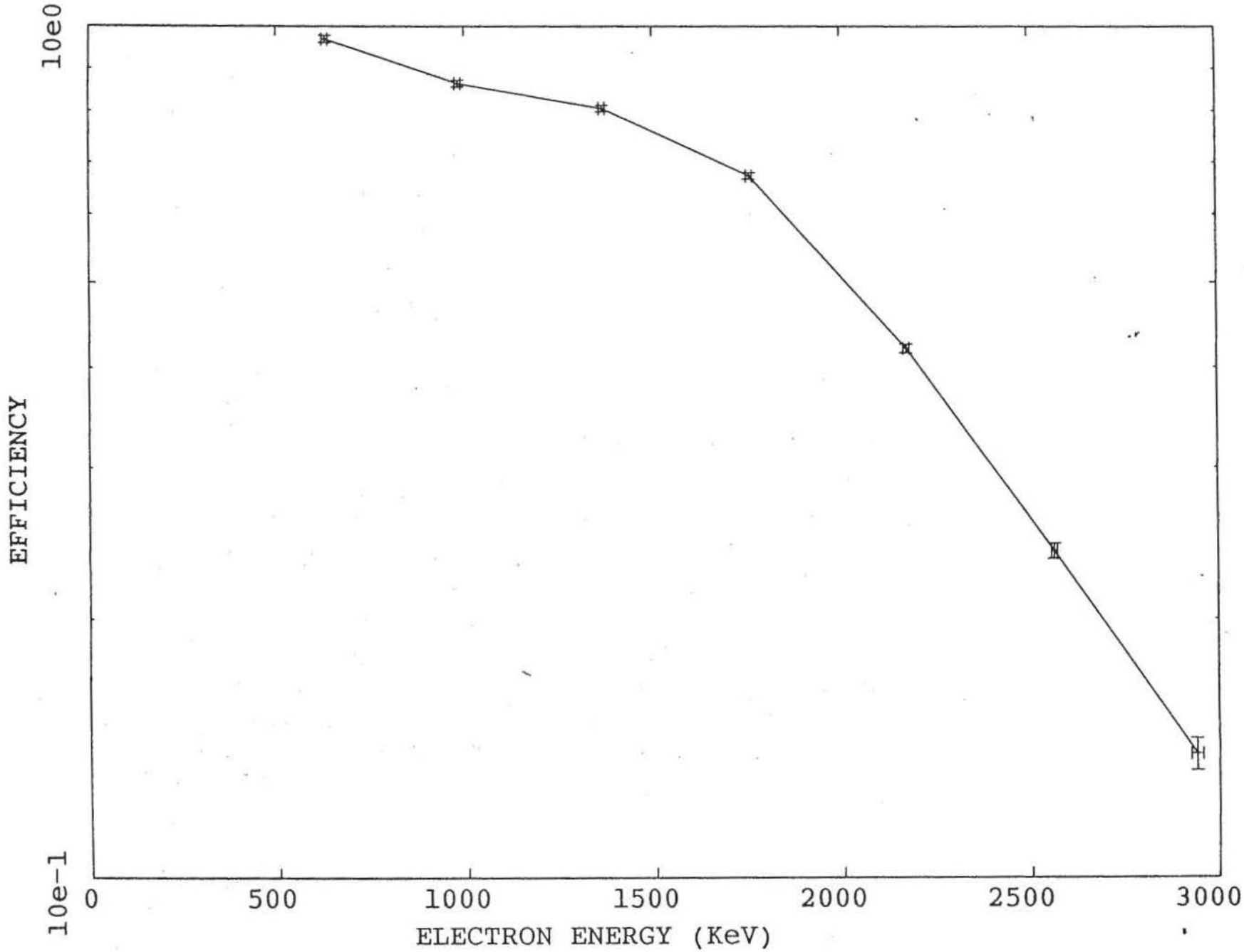

FIGURE 5: EFFICIENCY OF 450 MICRON DETECTOR (THRESHOLD=115KEV)

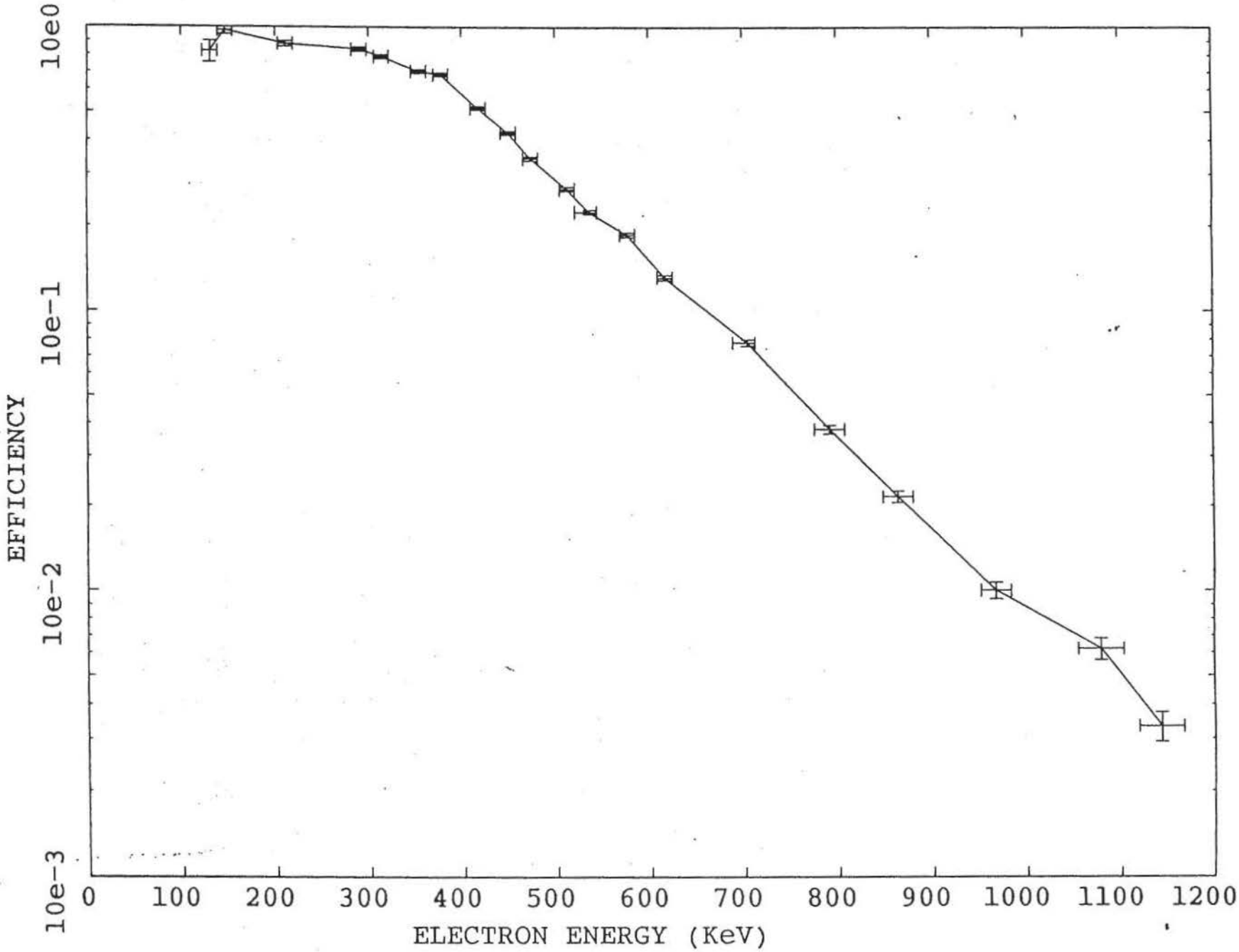

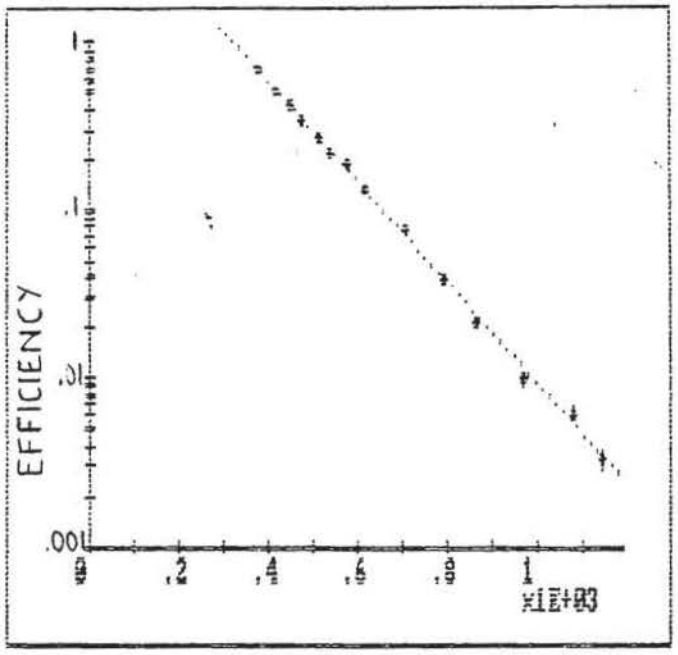

b:13eff

XOFF = 0
DX = 1000
YOFF = .001

Y = D*EXP(E*X)
(N = 14)
D = 9.263662
SIG(D) = .2283908
E = -6.892789E-03
SIG(E) = 4.686858E-05
CHI^2/(N-2) =
3.557651

efficiency vs. energy (normal incidence)

FIGURE 6

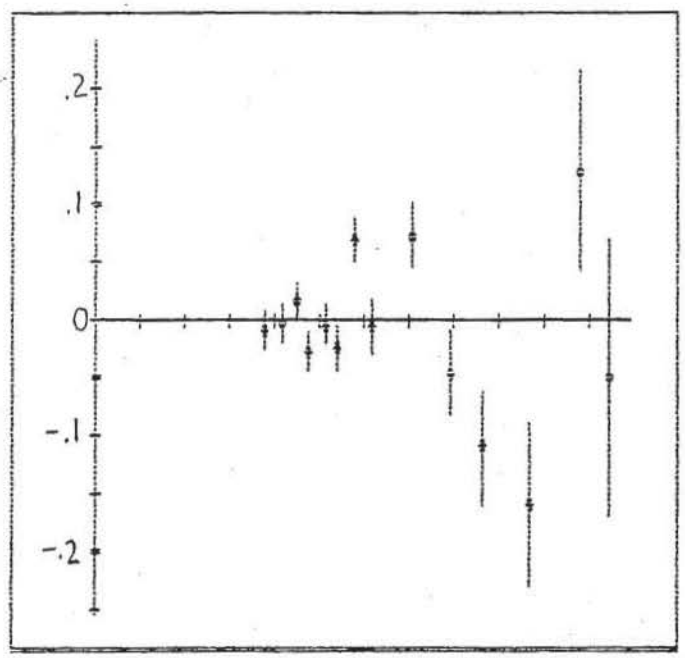

b:13eff

XOFF = 0
DX = 1000
YOFF = 0
DY = .05

difference plot---efficiency vs. energy (normal incidence)

FIGURE 7

FIGURE 8: ELECTRON ENERGY LOSS DISTRIBUTION IN 3 MM DETECTOR

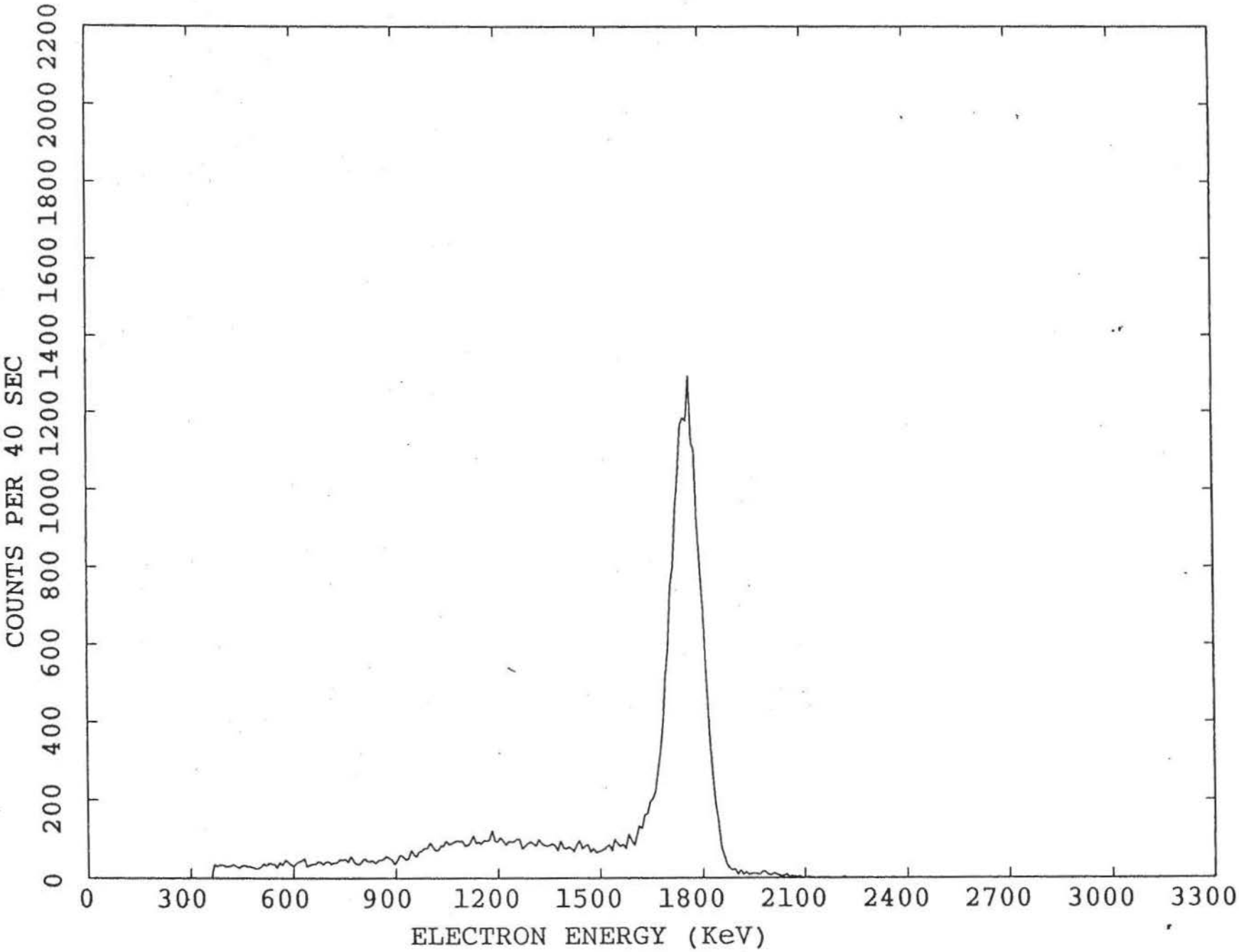

FIGURE 9: ELECTRON ENERGY LOSS DISTRIBUTION IN 3 MM DETECTOR

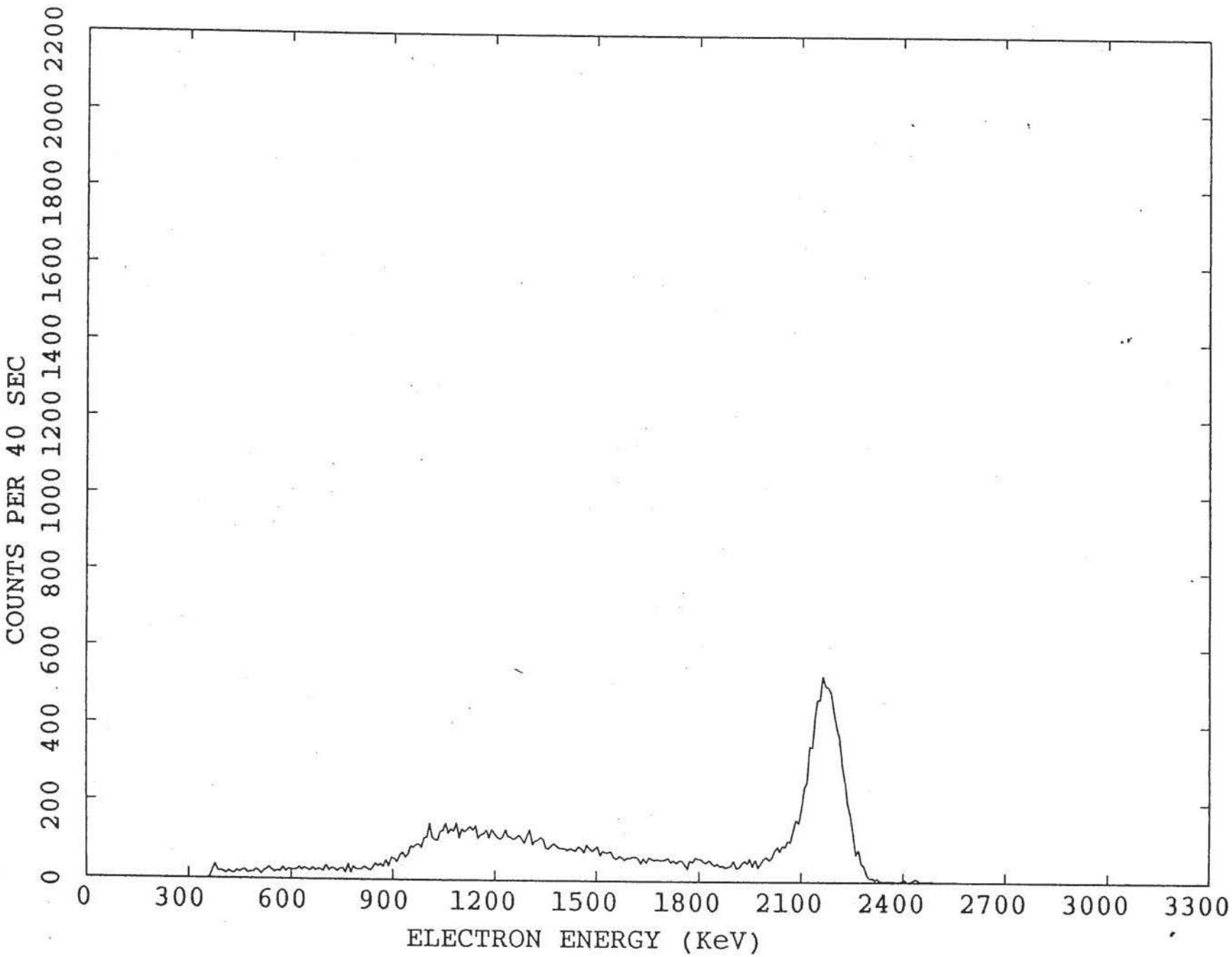

FIGURE 9B: ELECTRON ENERGY LOSS DISTRIBUTION IN 3 MM DETECTOR

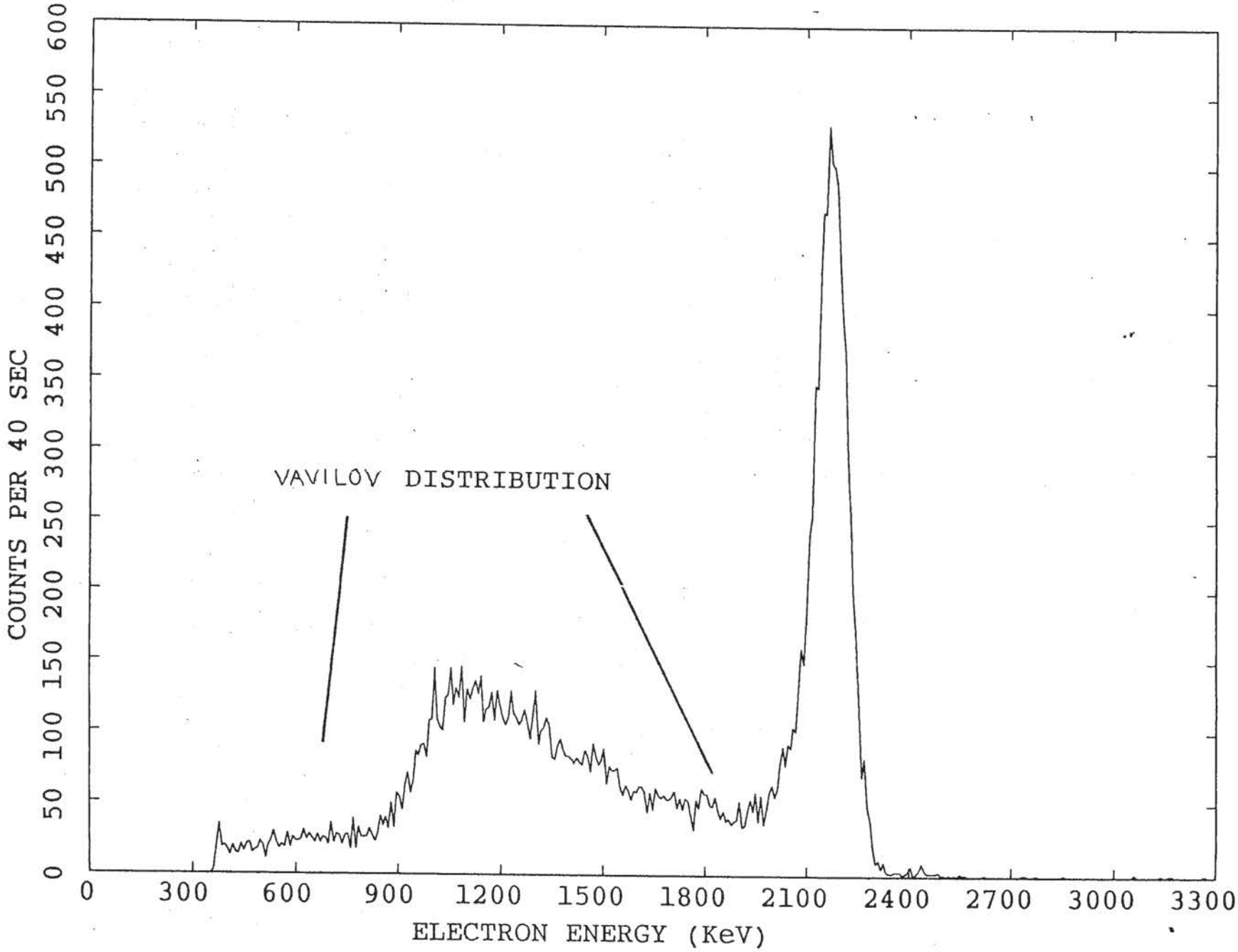

FIGURE 10: ELECTRON ENERGY LOSS DISTRIBUTION IN 3 MM DETECTOR

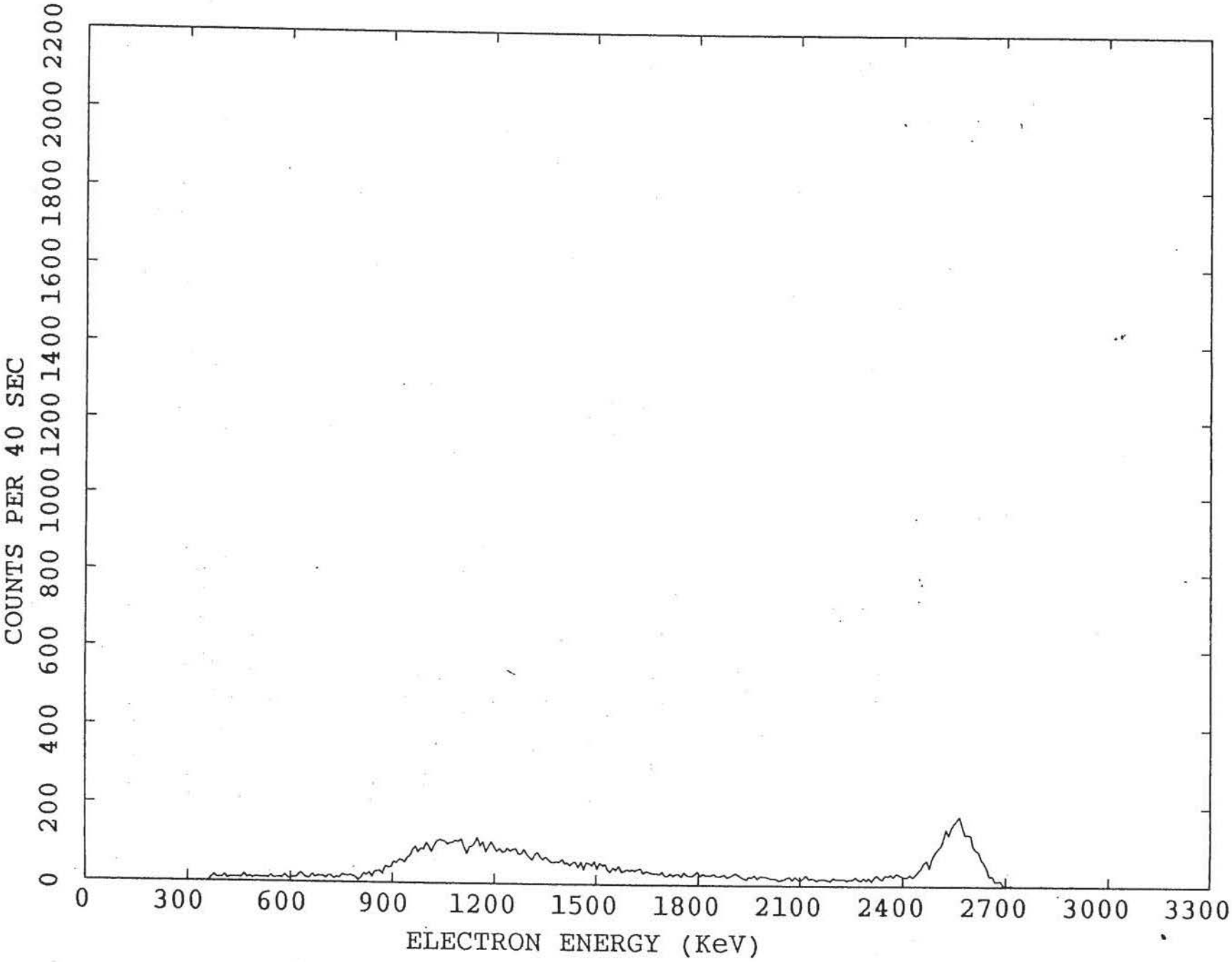

FIGURE 10B: ELECTRON ENERGY LOSS DISTRIBUTION IN 3 MM DETECTOR

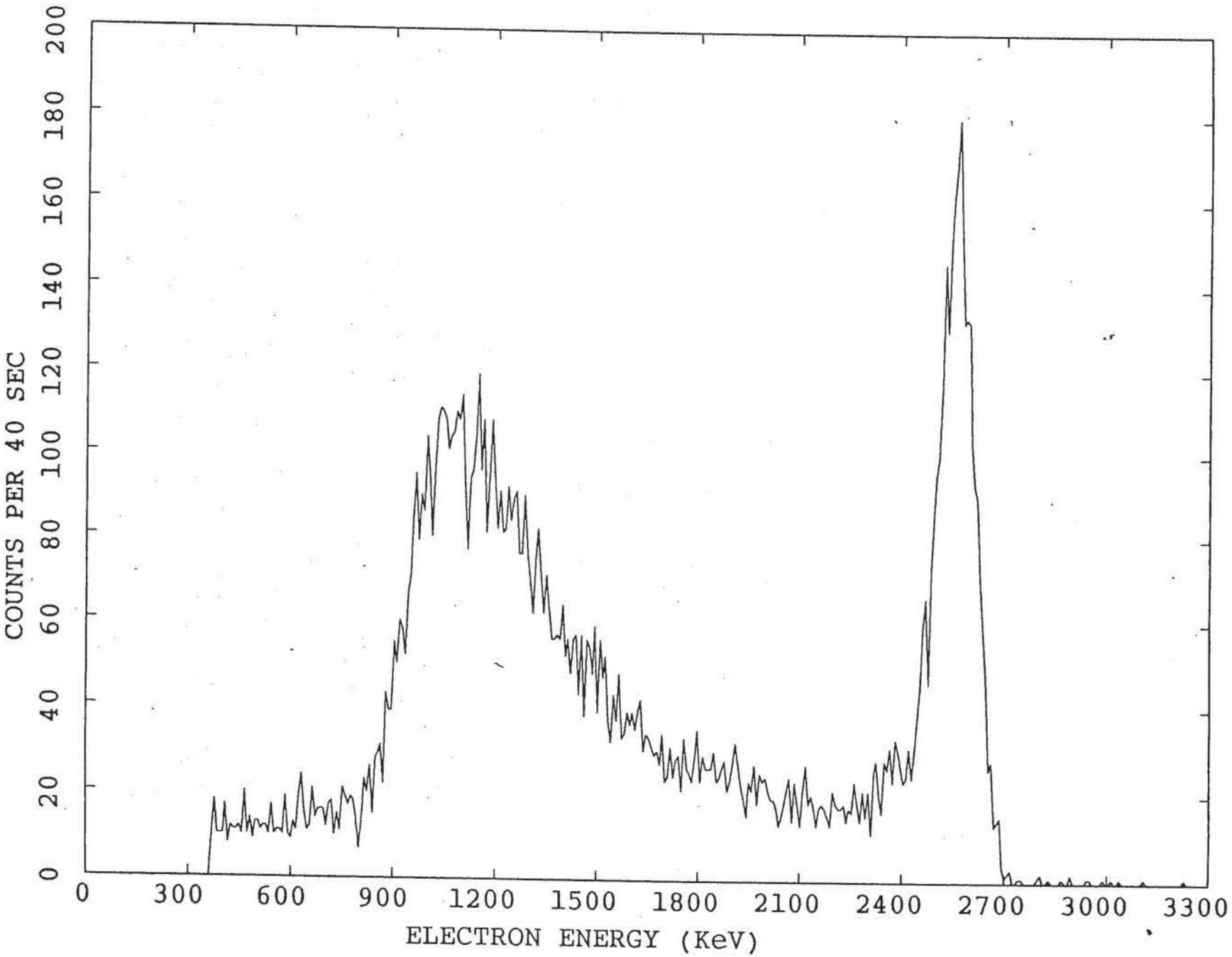

FIGURE 11: ELECTRON ENERGY LOSS DISTRIBUTION IN 3 MM DETECTOR

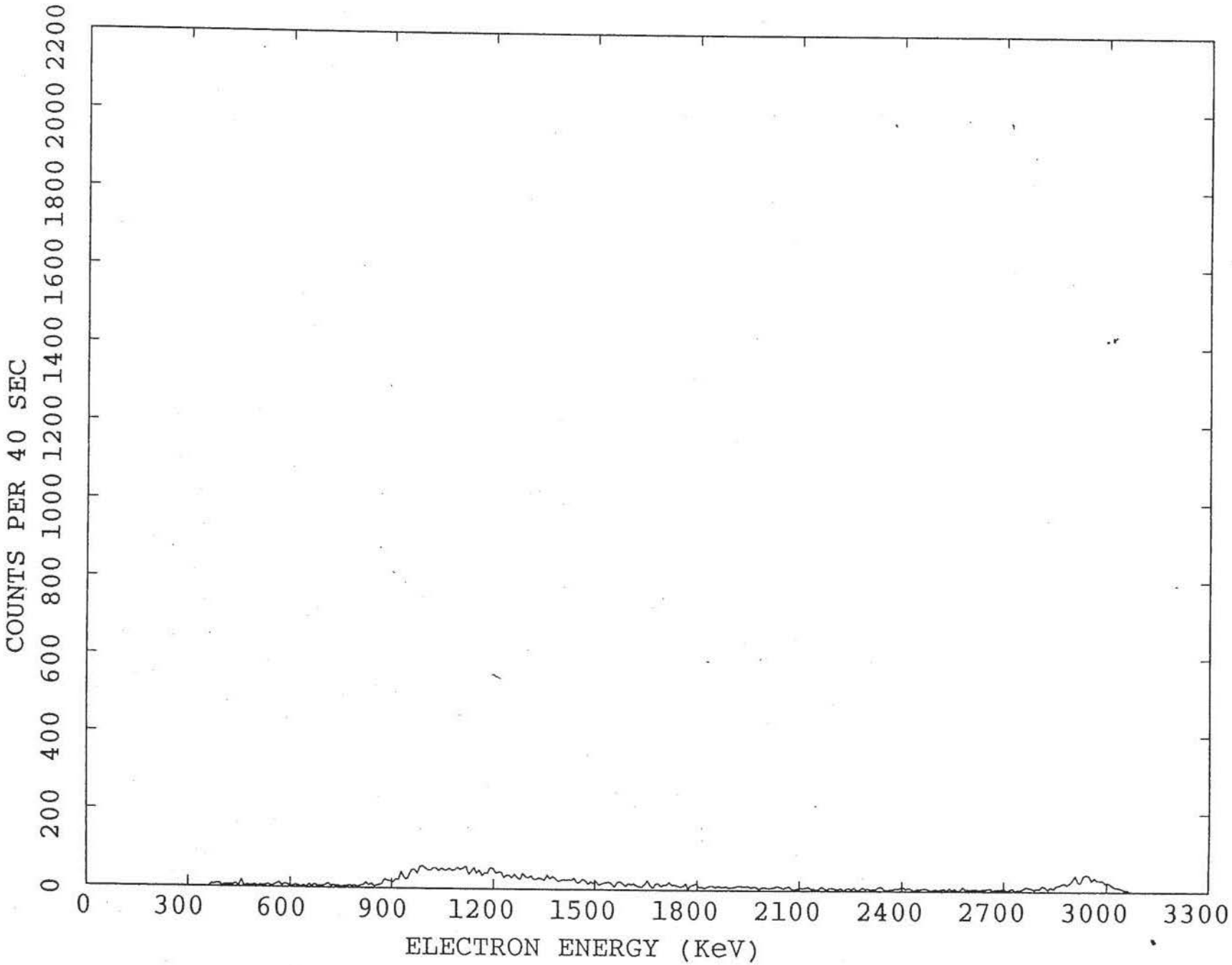

FIGURE 11B: ELECTRON ENERGY LOSS DISTRIBUTION IN 3 MM DETECTOR